# Parametrically excited helicopter ground resonance dynamics with high blade asymmetries

Leonardo Sanches, Guilhem Michon, Alain Berlioz, Daniel Alazard

# Parametrically Excited Helicopter Ground Resonance Dynamics With High Blade Asymmetries

L. Sanches[a,*], G. Michon[a], A. Berlioz[b], D. Alazard[c]

[a] *Université Toulouse, ICA, ISAE, 10 av. Edouard Belin, 31055 Toulouse, France*
[b] *Université Toulouse, ICA, UPS, 118 route de Narbonne, 31077 Toulouse, France*
[c] *Université Toulouse, DMIA, ISAE, 10 av. Edouard Belin, 31055 Toulouse, France*

**Abstract**

The present work is aimed at verifying the influence of high asymmetries in the variation of in-plane lead-lag stiffness of one blade on the ground resonance phenomenon in helicopters. The periodical equations of motions are analyzed by using Floquet's Theory (FM) and the boundaries of instabilities predicted. The stability chart obtained as a function of asymmetry parameters and rotor speed reveals a complex evolution of critical zones and the existence of bifurcation points at low rotor speed values. Additionally, it is known that when treated as parametric excitations; periodic terms may cause parametric resonances in dynamic systems, some of which can become unstable. Therefore, the helicopter is later considered as a parametrically excited system and the equations are treated analytically by applying the Method of Multiple Scales (MMS). A stability analysis is used to verify the existence of unstable parametric resonances with first and second order sets of equations. The results are compared and validated with those obtained by Floquet's Theory. Moreover, an explanation is given for the presence of unstable motion at low rotor speeds due to parametric instabilities of the second order.

*Keywords:* Nonlinear Dynamics, Floquet's Method, Method of Multiple Scales, Ground Resonance, Anisotropic Rotor

## Nomenclature

*Corresponding Author
*Email address:* leonardo.sanches@isae.fr (L. Sanches )

| Symbol | Description | Units |
|---|---|---|
| $a$ | Rotor eccentricity | m |
| $b$ | Blade equivalent length | m |
| [c.c.] | Complex conjugate terms | |
| $D_n^p$ | $\frac{\partial^p}{\partial T_n^p}$ - partial derivative with respect to time scales | |
| $\mathbf{F}_{ext}$ | External force vector | |
| $\mathbf{G}$ | Damping matrix of the dynamical system | |
| $I$ | Imaginary unit | |
| $I_{Zbk}$ | Lag rotational inertia of the k$^{\text{th}}$ blade around its center of gravity | kg m$^2$ |
| $\mathbf{K}$ | Stiffness matrix of the dynamical system | |
| $K_{bk}$ | k$^{\text{th}}$ blade lead-lag stiffness | N m rad$^{-1}$ |
| $K_{fX}$, $K_{fY}$ | Longitudinal and transverse stiffness of fuselage | N m$^{-1}$ |
| $m_f$, $m_{bk}$ | Fuselage and mass of k$^{\text{th}}$ blade | kg |
| $\mathbf{M}$ | Mass matrix of the dynamical system | |
| $N_b$ | Number of blades in the rotor | |
| $P(\Gamma, \sigma)$ | Characteristic polynomial equation | |
| $r_{ak}$ | $\sqrt{a\, r_{bk}}$ | |
| $r_{bk}$ | Ratio between the static moment over the total lead-lag rotational inertia of the k$^{\text{th}}$ blade | m$^{-1}$ |
| $r_{mk}$ | Ratio between the static moment of the k$^{\text{th}}$ blade over the total mass of the helicopter | m |
| $\mathbf{S}$ | State Space matrix | |
| $t$ | Time | s |
| $T_0$, $T_1$ | Time scales | s |
| $\mathbf{u}$ | Vector of degree of freedom of the system | |
| $\mathbf{v}$ | State variable vector | |
| $x(t)$ , $y(t)$ | Longitudinal and transverse displacement of the fuselage | m |
| $x_{bx}$, $y_{bx}$ | Blade position in x and y directions | m |
| $(x, y, z)$ | Mobile coordinate system attached to the rotor hub | |
| $(X_0, Y_0, Z_0)$ | Inertial referential coordinate system | |
| Greek Letters | | |

| | | |
|---|---|---|
| $\epsilon$ | Bookkeeping parameter | |
| $\varphi_k(t)$ | Lead-lag angle of $k^{th}$ blade | rad |
| $\Phi$ | Transition Matrix (Floquet's Theory) | |
| $\Gamma$ | Solutions of the characteristic polynomial equation | |
| $\lambda$ | Characteristic exponents | |
| $\Omega$ | Rotor speed | $\mathrm{rad\,s^{-1}}$ |
| $\sigma$ | Frequency detuning parameter | $\mathrm{rad\,s^{-1}}$ |
| $\zeta_k$ | Azimuth angle for the $k^{th}$ blade | rad |
| $\omega_{1..6}$ | Six natural frequencies of Eq.(8) | $\mathrm{rad\,s^{-1}}$ |
| $\omega_{b\,k}$ | Lead-lag natural frequencies of $k^{th}$ blade at rest, $k = 1..4$ | $\mathrm{rad\,s^{-1}}$ |
| $\omega_x$, $\omega_y$ | Fuselage resonance frequencies in x and y directions | $\mathrm{rad\,s^{-1}}$ |

## 1. Introduction

Perturbation methods have been dedicated to calculating differential equations with periodic, parametric and/or nonlinear terms. Hill's Infinite Determinant, Harmonic Balance Method and Method of Multiple Scales (MMS) are methods frequently employed to treat them [1, 2]. The reasons for using these methods are the need to obtain analytical expressions whose analysis is relatively simple and less computer time-consuming than numerical methods.

Nonlinear rotor dynamics [3, 4, 5], industrial problems with parametric excitations [6] and classical examples, e.g. pendulum dynamics in parametric excitations [7, 8, 9] are all examples of problems in which these methods have been used. In the latter applications, the authors observed that parametric excitations lead to the occurrence of parametric resonances that in turn lead to unstable oscillation conditions.

Research into the problem of the ground resonance phenomenon in helicopters was first performed by Coleman and Feingold [10]. Later, investigations on the occurrences of ground resonance for articulated, hingeless and bearingless rotors were carried out [11, 12, 13]. In all cases, the use of linearized periodic equations of motion provides very accurate frequency prediction of critical zones but only isotropic rotor configurations (all blades having the same properties) were analyzed.

The effects of geometric nonlinearities and the use of nonlinear springs

on the prediction of instabilities was verified [14, 15] with the application of perturbation methods.

Moreover, the dynamics of a helicopter subject to ground resonance, taking into account blade dissimilarities was examinated [16]. The results obtained by using Floquet's Theory confirm that the introduction of slight asymmetry $\pm 5\%$ on the in-plane lead-lag stiffness of one blade shifts the boundary speeds of unstable regions, making them wider.

The present work is aimed at verifying the influence of high in-plane stiffness variation at one blade on the stability of the ground resonance phenomenon. The presence of viscous damping is not considered in the mechanical model, in order to highlight all the possible instabilities. Firstly, by using Floquet's Theory, the boundaries of stability are determined as a function of the asymmetry parameter and rotor speed. Following this, by considering the helicopter as a parametrically excited system, the equations are solved by using the MMS.

The dynamical equations of motion from the mechanical model are formulated in section 2 while sections 3 and 4 describe the methodologies applied to the set of periodic motion equations, namely the Floquet Method (FM) and the MMS. The critical rotor speeds predicted by both methods are presented in section 5 and compared for an anisotropic rotor configuration.

## 2. Derivation of Equations

Figure 1 provides a general diagram of the dynamical system. It represents a simplified helicopter model very similar to that proposed by the earliest research in aeromechanical stability [10], e.g. the ground resonance phenomenon.

Considered as a rigid body the fuselage has a longitudinal $x(t)$ and a lateral $y(t)$ displacement, respectively. The flexibility of the landing skid is represented by springs placed in both directions. At its rest point, the center of mass (point $O$) of the fuselage is coincident with the origin of an inertial coordinate system ($X_0$, $Y_0$, $Z_0$).

The rotor head system consists of an assembly of one rigid rotor hub with $N_b$ blades. Each $k$ blade is represented by a concentrated mass and has an in-plane lead-lag motion defined by $\varphi_k(t)$. Length $b$ is the radius of gyration, i.e. the distance from the articulation at point $B$ and the concentrated mass assuming an equivalent rotational inertia of a blade. The stiffness of the

lead-lag blade motion is provided by a torsional spring presented at each articulation.

The origin of a mobile coordinate system ($x$, $y$, $z$) parallel to the inertial system is located at the geometric center of the rotor hub (point $A$). The rotor revolves at speed $\Omega$.

Both body and rotor head are joined by a rigid shaft. Neither aerodynamic forces on the blades nor viscous damping are considered.

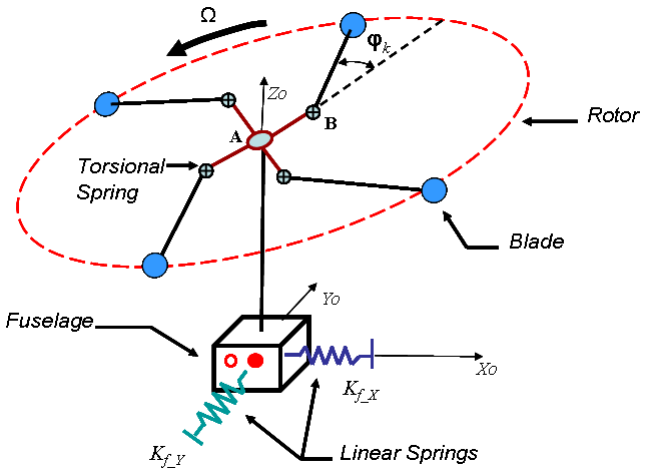


Figure 1: Schema of the mechanical system

Moreover, the following conditions are considered.

- The fuselage has a mass $m_f$ and spring stiffness $K_{f\,X}$ and $K_{f\,Y}$ linked to it through directions $x$ and $y$, respectively;
- The rotor is composed of $N_b = 4$ blades and each blade $k$ has an azimuth angle of $\zeta_k = 2\pi\,(k-1)\,/N_b$ with the $x$ - axis;
- Each blade has the same mass $m_{b\,k}$ and moment of inertia $I_{z\,b\,k}$ around the $z$ - axis ;
- The angular spring constant for each blade $k$ is $K_{b\,k}$;
- The position of blade $k$ projected in the inertial coordinate system is:

$$x_{b\,k} = a\cos\left(\Omega t + \zeta_k\right) + b\cos\left(\Omega t + \zeta_k + \varphi_k(t)\right) + x(t)$$

$$y_{b\,k} = a\sin\left(\Omega t + \zeta_k\right) + b\sin\left(\Omega t + \zeta_k + \varphi_k(t)\right) + y(t)$$

where $a$ is rotor eccentricity (i.e. hinge offset).

The vector of degrees of freedom of the system is obtained by considering the general Laplace variable $\mathbf{u}$ as:

$$\mathbf{u}_{1..6}\left(t\right) = \left\{ \begin{array}{cccccc} x(t) & y(t) & \varphi_1(t) & \varphi_2(t) & \varphi_3(t) & \varphi_4(t) \end{array} \right\}$$

The Lagrange equation is introduced in the kinetic and the potential energy expressions of the system (body and rotor) and equations of motion are obtained. Later, the nonlinear terms are neglected and a first order Taylor series expansion for the trigonometric blade lead-lag angle terms is performed.

The linear matrix equation of motion of the dynamical system obtained is:

$$\mathbf{M}\,\ddot{\mathbf{u}} + \mathbf{G}\,\dot{\mathbf{u}} + \mathbf{K}\,\mathbf{u} = \mathbf{F}_{ext} \tag{1}$$

$\mathbf{M}$, $\mathbf{G}$ and $\mathbf{K}$ correspond to the mass, damping and stiffness matrices, respectively. They are non-symmetric and non-diagonal matrices due to the presence of periodic terms. Moreover, $\mathbf{F}_{ext}$ is equal to zero for blades with the same inertial and geometrical properties. They are all expressed in Eq.(2) to Eq.(5), as follows:

$$\mathbf{M}(t) = \begin{bmatrix} 1 & 0 & -r_{m1}\sin(\psi_1) & -r_{m2}\sin(\psi_2) & -r_{m3}\sin(\psi_3) & -r_{m4}\sin(\psi_4) \\ 0 & 1 & r_{m1}\cos(\psi_1) & r_{m2}\cos(\psi_2) & r_{m3}\cos(\psi_3) & r_{m4}\cos(\psi_4) \\ -r_{b1}\sin(\psi_1) & r_{b1}\cos(\psi_1) & 1 & 0 & 0 & 0 \\ -r_{b2}\sin(\psi_2) & r_{b2}\cos(\psi_2) & 0 & 1 & 0 & 0 \\ -r_{b3}\sin(\psi_3) & r_{b3}\cos(\psi_3) & 0 & 0 & 1 & 0 \\ -r_{b4}\sin(\psi_4) & r_{b4}\cos(\psi_4) & 0 & 0 & 0 & 1 \end{bmatrix} \tag{2}$$

$$\mathbf{G}(t) = \begin{bmatrix} 0 & 0 & -2\Omega r_{m1}\cos(\psi_1) & -2\Omega r_{m2}\cos(\psi_2) & -2\Omega r_{m3}\cos(\psi_3) & -2\Omega r_{m4}\cos(\psi_4) \\ 0 & 0 & -2\Omega r_{m1}\sin(\psi_1) & -2\Omega r_{m2}\sin(\psi_2) & -2\Omega r_{m3}\sin(\psi_3) & -2\Omega r_{m4}\sin(\psi_4) \\ 0 & 0 & 0 & 0 & 0 & 0 \\ 0 & 0 & 0 & 0 & 0 & 0 \\ 0 & 0 & 0 & 0 & 0 & 0 \\ 0 & 0 & 0 & 0 & 0 & 0 \end{bmatrix} \tag{3}$$

$$\mathbf{K}(t) = \begin{bmatrix} \omega_x^2 & 0 & \Omega^2 r_{m1}\sin(\psi_1) & \Omega^2 r_{m2}\sin(\psi_2) & \Omega^2 r_{m3}\sin(\psi_3) & \Omega^2 r_{m4}\sin(\psi_4) \\ 0 & \omega_y^2 & -\Omega^2 r_{m1}\cos(\psi_1) & -\Omega^2 r_{m2}\cos(\psi_2) & -\Omega^2 r_{m3}\cos(\psi_3) & -\Omega^2 r_{m4}\cos(\psi_4) \\ 0 & 0 & \omega_{b\,1}^2 + \Omega^2 r_{a\,1}^2 & 0 & 0 & 0 \\ 0 & 0 & 0 & \omega_{b\,2}^2 + \Omega^2 r_{a\,2}^2 & 0 & 0 \\ 0 & 0 & 0 & 0 & \omega_{b\,3}^2 + \Omega^2 r_{a\,3}^2 & 0 \\ 0 & 0 & 0 & 0 & 0 & \omega_{b\,4}^2 + \Omega^2 r_{a\,4}^2 \end{bmatrix} \tag{4}$$

$$\mathbf{F}_{ext}(t) = \begin{bmatrix} \sum_{k=1}^{N_b} \Omega^2 r_{m\,k} \left(\frac{a+b}{a}\right) \cos(\psi_k) \\ \sum_{k=1}^{N_b} \Omega^2 r_{m\,k} \left(\frac{a+b}{a}\right) \sin(\psi_k) \\ 0 \\ 0 \\ 0 \\ 0 \end{bmatrix} \tag{5}$$

where

$r_{m\,k} = \frac{b\, m_{b\,k}}{m_f + \sum_{k=1}^{N_b} m_{b\,k}}$, $r_{b\,k} = \frac{b\, m_{b\,k}}{b^2\, m_{b\,k} + I_{z_{b\,k}}}$, $r_{a\,k}^2 = a\, r_{b\,k}$, $\psi_k = \Omega t + \zeta_k$,

$\omega_x^2 = \frac{K_{f\,X}}{m_f + \sum_{k=1}^{N_b} m_{b\,k}}$, $\omega_y^2 = \frac{K_{f\,Y}}{m_f + \sum_{k=1}^{N_b} m_{b\,k}}$, $\omega_{b\,k}^2 = \frac{K_{b\,k}}{b^2\, m_{b\,k} + I_{z_{b\,k}}}$ $k$=1..$N_b$

Factors $r_{m\,k}$ and $r_{b\,k}$ representing the ratio between the blade static moment over the total translatory inertia of the helicopter and the total rotational inertia of the blade, respectively, are small when compared to the unit.

Terms $\omega_x$ and $\omega_y$ are the natural frequencies of the fuselage in directions $x$ and $y$, respectively. Moreover, $\omega_{b\,1..4}$ are the lead-lag natural frequencies of blades 1 to 4 at rest.

## 3. Floquet's Method

A stability analysis of the periodic equations of motion is carried out by using Floquet's theory [17, 18, 19]. This permits predetermining the critical rotor speeds at which the ground resonance phenomenon occurs.

In order to attain this objective, the dynamical system in Eq.(1) is represented in a state-space form as:

$$\dot{\mathbf{v}}(t) = \mathbf{S}(t)\, \mathbf{v}(t),\ t > t_0$$
$$\mathbf{v}(t) = \mathbf{v}_0,\ \mathbf{v}(t) = \begin{bmatrix} \mathbf{u}(t) & \dot{\mathbf{u}}(t) \end{bmatrix}^T$$

where $\mathbf{S}(t)$ is the state-space matrix with period $T$ and $\mathbf{v}(t)$ is the state variable vector.

According to Floquet's Theory, there is a transition matrix $\mathbf{\Phi}$ that links $\mathbf{v}(t_0)$ to $\mathbf{v}(t)$ and is defined as: $\mathbf{\Phi}(t, t_0) = \mathbf{P}(t, t_0)\, \mathrm{e}^{\mathbf{Q}(t-t_0)}$.

The monodromy matrix $\mathbf{R}$ or the Floquet Transition Matrix (FTM) defined as:

$$\mathbf{R} = \mathbf{\Phi}(t_0 + T,\, t_0)$$

is computed by admitting the periodic system matrices, Eq.(1), as a switched periodical system. As reported by Dufour [20], matrix $\mathbf{S}(t)$ is approximated by a series of $p$ step functions and the monodromy matrix can be obtained as follows:

$$\mathbf{R} = \prod_{k=1}^{p} \mathrm{e}^{\mathbf{S}_k (t_k - t_{k-1})} \tag{6}$$

where matrix $\mathbf{S}_k$, within the interval defined by $t_k$ and $t_{k-1}$, is constant value of $\mathbf{S}(t)$ at $t = t_{k-1}$.

The dynamical system Eq.(1) is exponentially stable if $\mathbf{R}$ is Schur. This means that if all the norms of the eigenvalues of $\mathbf{R}$, known as characteristic multipliers, are less than one.

## 4. Method of Multiple Scales

The Method of Multiple Scales is applied in order to treat the periodic equations of motion analytically. Apart from this application, the present method has been frequently employed in nonlinear industrial problems [6] and nonlinear rotating machines [3, 4, 5].

In the present work, great attention is paid to parametrically excited systems [7, 9]. The presence of parametric and periodic terms can subject the system to parametric instability conditions.

By introducing the bookkeeping parameter $\epsilon$ into the expansion of any time dependent functions having the form:

$$\begin{aligned} \mathbf{u}_n(t) \;&= \mathbf{u}_{n_0}(T_0, T_1, T_2) + \epsilon\, \mathbf{u}_{n_1}(T_0, T_1, T_2) + \\ &\quad \epsilon^2\, \mathbf{u}_{n_2}(T_0, T_1, T_2) + \mathcal{O}(3),\; n = 1..6 \end{aligned} \tag{7}$$

and by scaling the periodic terms to appear as parametric excitations at the first order of $\epsilon$ by considering $r_{m\,k} = \epsilon \alpha_k$ and $r_{b\,k} = \epsilon \beta_k$, three sets of equations are obtained by grouping them as a function of the power of $\epsilon$ once Eq.(7) is replaced in Eq.(1).

Note that $T_n = \epsilon^n t$, $n \in \mathbb{R}+$ are time scales and terms with a higher order than $\epsilon^3$ are neglected.

*4.1. Order $\epsilon^{\mathbf{0}}$ equations*

The set of order $\epsilon^0$ equations collected is:

$$\mathrm{D}_0^2\, u_{n_0} + \omega_n^2\; u_{n_0} = 0,\; n = 1..6 \tag{8}$$

where $\mathrm{D}_0$ is the partial derivative with respect to $T_0$ and

$$\omega_1 = \omega_x,\; \omega_2 = \omega_y,\; \omega_{k+2} = \sqrt{\omega_{b\,k}^2 + r_{a\,k}^2 \Omega^2},\;\; k = 1..N_b$$

The six equations of motion are homogeneous and independent which indicates dynamic uncoupling between rotor and fuselage dynamics on the fast time scale. The solutions of these equations are trivial and take the form $u_{n_0} = \frac{1}{2} C_n\left(T_1, T_2\right) \mathrm{e}^{(I\,\omega_n T_0)} + [c.c.]\,,\; n$=1..6. The term $C_n\left(T_1, T_2\right)$ is complex and [c.c.] represents the complex conjugate of the previous terms.

*4.2. Order $\epsilon^{\mathbf{1}}$ equations*

The set equations of order $\epsilon^1$ are represented below.

$$\begin{aligned} &\mathrm{D}_0^2 u_{1_1} + \omega_1^2\, u_{1_1} = -2\mathrm{D}_1\mathrm{D}_0 u_{1_0} + \\ &\quad \sum_{n=3}^{6} \left\{ \begin{array}{c} -\frac{1}{2} I^{(n-2)} \alpha_{n-2} \mathrm{D}_0^2\, u_{n_0} \mathrm{e}^{(I\Omega T_0)} + I^{(n-3)} \alpha_{n-2} \Omega \mathrm{D}_0\, u_{n_0} \mathrm{e}^{(I\Omega T_0)} \\ +\frac{1}{2} I^{(n-2)} \alpha_{n-2} \Omega^2\, u_{n_0} \mathrm{e}^{(I\Omega T_0)} + [c.c.] \end{array} \right\} \end{aligned} \tag{9}$$

$$\begin{aligned} &\mathrm{D}_0^2 u_{2_1} + \omega_2^2\, u_{2_1} = -2\mathrm{D}_1\mathrm{D}_0 u_{2_0} + \\ &\quad \sum_{n=3}^{6} \left\{ \begin{array}{c} -\frac{1}{2}\, I^{(n-3)} \alpha_{n-2} \mathrm{D}_0^2\, u_{n_0} \mathrm{e}^{(I\Omega T_0)} - I^{(n-2)} \alpha_{n-2} \Omega \mathrm{D}_0\, u_{n_0} \mathrm{e}^{(I\Omega T_0)} \\ +\frac{1}{2}\, I^{(n-3)} \alpha_{n-2} \Omega^2\, u_{n_0} \mathrm{e}^{(I\Omega T_0)} + [c.c.] \end{array} \right\} \end{aligned} \tag{10}$$

$$\begin{aligned} \mathrm{D}_0^2 u_{n_1} + \omega_n^2\, u_{n_1} = &-2\mathrm{D}_1\mathrm{D}_0 u_{n_0} + \\ &- \frac{1}{2} I^{(n-2)} \beta_{n-2} \mathrm{D}_0^2\, u_{1_0} \mathrm{e}^{(I\Omega T_0)} \\ &- \frac{1}{2} I^{(n-3)} \beta_{n-2} \mathrm{D}_0^2\, u_{2_0} \mathrm{e}^{(I\Omega T_0)} + [c.c.]\,,\; n = 3..6 \end{aligned} \tag{11}$$

The right-hand side of the above equations highlights the existence of external excitations that are totally dependent on the steady-state responses $u_{n_0}$. The responses $u_{n_0}$ are time dependent of $T_0$, $T_1$ and $T_2$.

*4.2.1. Parametric Resonances of first order - $\epsilon^{\mathbf{1}}$ equations*

The external excitations on equations of order $\epsilon^1$, manifested by the presence of $u_{n_0}\mathrm{e}^{(I\Omega T_0)}$ and/or its variation, lead the dynamical system to a resonance condition depending on the rotor speed value attributed for $\Omega$. The resonance is detected when any combination of frequencies of exciting terms becomes equal to the natural frequencies of the linear dynamical system.

To clarify the procedure, the combination of frequencies are represented below once the solutions of Eq.(8) are substituted in Eq.(9) to Eq.(11) and the exponential terms collected.

Body Equations - Eq.(9) and Eq.(10):

$$[\,|\Omega \pm \omega_n|\,],\ n = 3..6 \tag{12}$$

Blade Equations - Eq.(11):

$$\left[\ |\Omega \pm \omega_1| \quad |\Omega \pm \omega_2|\ \right] \tag{13}$$

Submitting Eq.(12) equal to $\omega_1$ and $\omega_2$ and Eq.(13) equal to $\omega_{3..6}$, the rotor speeds at which a resonance occurs are:

Body equation - Eq.(9):

$$\left[\ |\omega_1 \pm \omega_3| \quad |\omega_1 \pm \omega_4| \quad |\omega_1 \pm \omega_5| \quad |\omega_1 \pm \omega_6|\ \right] \tag{14}$$

Body equation - Eq.(10):

$$\left[\ |\omega_2 \pm \omega_3| \quad |\omega_2 \pm \omega_4| \quad |\omega_2 \pm \omega_5| \quad |\omega_2 \pm \omega_6|\ \right] \tag{15}$$

Blade equations - Eq.(11):

$$\left[\ |\omega_1 \pm \omega_n| \quad |\omega_2 \pm \omega_n|\ \right],\ n = 3..6 \tag{16}$$

Under this condition, the resonant terms are considered as secular terms [1, 2].

*4.2.2. Solvability Conditions - $\epsilon^{\mathbf{1}}$ equations*

In order to obtain solutions for the inhomogeneous equations, certain solvability conditions must be satisfied when using asymptotic or perturbation methods. Particularly with MMS, the secular terms should be eliminated by setting their coefficients equal to zero. A set of so-called solvability equations is obtained. Their solutions lead to determining specific conditions and the

relation between the amplitude responses of motion of the previous order of the $\epsilon$ dynamical system.

In the present work, emphasis is given to studying the stability of such equations. This entails predicting the ground resonance phenomenon by determining the boundary speeds of unstable zones for any type of rotor.

For this reason, a detuning frequency parameter $\sigma$ is introduced into the harmonic terms before scaling the equations of motion in Eq.(1). Considering $\Omega = \Omega_R + \epsilon\sigma$ permits controlling the nearness of a resonance case identified by $\Omega_R$ and shown in Eqs.(14) to (16).

The secular terms are collected once the value of $\Omega_R$ has been substituted in the new $\epsilon^1$ set of equations. Six linear differential equations, known as solvability equations, are obtained. They are a function of the complex amplitudes $C_n\,(T_1, T_2)$ and/or its conjugate $\overline{C_n}\,(T_1, T_2)$, $n = 1..6$.

*4.2.3. Non Resonant Case – $\epsilon^1$ equations*

A non resonant case at $\epsilon^1$ equations is established when the $\Omega$ does not belong to the rotor speed values defined in Eqs.(14) to (16).

The solvability equations are therefore:

$$\frac{\partial}{\partial T_1} C_n\,(T_1, T_2) = 0, \;\; n = 1..6 \tag{17}$$

which lead the amplitude responses $C_n$ be independent of $T_1$.

Taking into account the above solvability conditions and replacing them in Eqs.(9) to (11), the responses $u_{n_1}\,(T_0, T_1, T_2)$ are obtained by solving the inhomogeneous second order differential equations (see Appendix A).

*4.3. Order $\epsilon^2$ equations*

The set of equations of order $\epsilon^2$ is:

$$\begin{aligned} \mathrm{D}_0^2 u_{1_2} + \omega_1^2\, u_{1_2} = & -2\,\mathrm{D}_2\mathrm{D}_0\, u_{1_0} - \mathrm{D}_1^2 u_{1_0} - 2\,\mathrm{D}_1\mathrm{D}_0 u_{1_1} \\ & \sum_{n=3}^{6} \left\{ \begin{array}{l} -I^{(n-2)}\alpha_{n-2}\left[\frac{1}{2}\mathrm{D}_0^2\, u_{n_1} + \mathrm{D}_1\mathrm{D}_0\, u_{n_0}\right] \mathrm{e}^{(I\Omega T_0)} \\ +I^{(n-3)}\Omega\,\alpha_{n-2}\left[\frac{1}{2}\mathrm{D}_0\, u_{n_1} + \mathrm{D}_1\, u_{n_0}\right] \mathrm{e}^{(I\Omega T_0)} \\ +\frac{1}{2}\, I^{(n-2)}\,\alpha_{n-2}\Omega^2\, u_{n_1}\mathrm{e}^{(I\Omega T_0)} + [c.c.] \end{array} \right\} \end{aligned} \tag{18}$$

$$\mathrm{D}_0^2 u_{2_2} + \omega_2^2\, u_{2_2} = -2\,\mathrm{D}_2\mathrm{D}_0\, u_{2_0} - \mathrm{D}_1^2 u_{2_0} - 2\,\mathrm{D}_1\mathrm{D}_0 u_{2_1}$$
$$\sum_{n=3}^{6} \left\{ \begin{array}{l} -I^{(n-3)}\alpha_{n-2}\left[\frac{1}{2}\mathrm{D}_0^2\, u_{n_1} + \mathrm{D}_1\mathrm{D}_0\, u_{n_0}\right] \mathrm{e}^{(I\Omega T_0)} \\ -I^{(n-2)}\Omega\,\alpha_{n-2}\left[\frac{1}{2}\mathrm{D}_0\, u_{n_1} + \mathrm{D}_1\, u_{n_0}\right] \mathrm{e}^{(I\Omega T_0)} \\ +\frac{1}{2}\, I^{(n-3)}\,\alpha_{n-2}\Omega^2\, u_{n_1} \mathrm{e}^{(I\Omega T_0)} + [c.c.] \end{array} \right\} \tag{19}$$

$$\begin{array}{l} \mathrm{D}_0^2 u_{n_2} + \omega_6^2\, u_{n_2} = -2\,\mathrm{D}_2\mathrm{D}_0\, u_{n_0} - \mathrm{D}_1^2 u_{n_0} - 2\,\mathrm{D}_1\mathrm{D}_0 u_{n_1} \\ -I^{(n-2)}\beta_{n-2}\left(\frac{1}{2}\mathrm{D}_0^2\, u_{1_1} + \mathrm{D}_1\mathrm{D}_0\, u_{1_0}\right) \mathrm{e}^{(I\Omega T_0)} \quad , n = 3..6 \\ -I^{(n-3)}\beta_{n-2}\left(\frac{1}{2}\mathrm{D}_0^2 u_{2_1} + \mathrm{D}_1\mathrm{D}_0\, u_{2_0}\right) \mathrm{e}^{(I\Omega T_0)} \end{array} \tag{20}$$

Note that $u_{n_0}$ and $u_{n_1}$ are time dependents of $T_0$, $T_1$ and $T_2$.

*4.3.1. Parametric Resonances of second order - $\epsilon^2$ equations*

The same procedure developed in section 4.2.1 is used to determine the parametric resonances of the second order. However, for this goal, the expressions of $u_{n_1}(T_0, T_1, T_2)$ are necessary.

It is assumed, for instance, that any parametric resonance of the second order is similar to those found in first order equations which leads to validating the responses determined in Appendix A. By substituting them, the solvability conditions found in section 4.2.3 and the responses of $u_{n_0}(T_0, T_1, T_2)$ in Eqs.(18) to (20), the combination of frequencies of the exciting terms at order $\epsilon^2$ equations are:

Body Equations - Eqs.(18) and (19):

$$|\pm 2\Omega \pm \omega_n|\ ,\ n = 1..2 \tag{21}$$

Blade Equations - Eq.(20):

$$|\pm 2\Omega \pm \omega_n|\ ,\ n = 3..6 \tag{22}$$

The rotor speeds at which a resonance of the second order occurs are calculated by making Eq.(21) equal to $\omega_1$ and $\omega_2$ and Eq.(22) equal to $\omega_{3..6}$. They are represented below as,

Body equation - Eq.(18):

$$|\omega_1|\,, \quad \left|\tfrac{\omega_i+\omega_j}{2}\right|, \quad \left|\tfrac{\omega_i-\omega_j}{2}\right| \quad i \neq j \rightarrow i\,,\, j = 1..2 \tag{23}$$

Body equation - Eq.(19):

$$|\omega_2|\,, \quad \left|\tfrac{\omega_i+\omega_j}{2}\right|, \quad \left|\tfrac{\omega_i-\omega_j}{2}\right| \quad i \neq j \rightarrow i\,,\, j = 1..2 \tag{24}$$

Blade equations - Eq.(20):

$$|\omega_i|\,, \quad \left|\tfrac{\omega_i+\omega_j}{2}\right|, \quad \left|\tfrac{\omega_i-\omega_j}{2}\right| \quad i \neq j \rightarrow i\,,\, j = 3..6 \tag{25}$$

*4.3.2. Solvability Conditions - $\epsilon^2$ equations*

The objective of this section is similar to that explained previously in section 4.2.2 and the same procedure is utilized. Nevertheless, in order to control the nearness of the parametric resonances of the second order, $\Omega = \Omega_R + \epsilon^2\sigma$ is considered before scaling the equations of motion in Eq.(1).

It should be noted that the solvability equations will be expressed as a function of complex amplitude $C_n\,(T_2)$ and/or its conjugate $\overline{C_n}\,(T_2)$, $n = 1..6$.

## 5. Study Case - Anisotropic Rotor

The study of the influence of asymmetric blades on helicopter stability is considered by examining the boundaries of the ground resonance phenomenon. Wang [16] verified the effect of the in-plane lead-lag stiffness variation of $\pm 5\%$ at one blade on the regressing lag mode stability for a Bousman 3-bladed rotor.

In this work, however, a wide range of in-plane lead-lag stiffness variations is considered by altering the lead-lag natural frequency in $\pm 100\%$. From a practical point of view, the dissimilarities between blades may exist due to the aging effects (i.e.: loss of mechanical properties) and/or rupture of mechanical elements. The $4^{\text{th}}$ blade is assumed to be dissimilar from the others and FM is applied.

Later, an anisotropic rotor case from those analyzed previously, is studied by considering the helicopter as a parametrically excited dynamic system. The unstable regions are predicted by MMS and the results are compared with those obtained by FM.

Table 1 exposes the reference data of the helicopter with isotropic rotor.

Table 1: Numerical values of the fuselage and rotor head inputs

| Fuselage | | Rotor | | |
|---|---|---|---|---|
| $m_f = 2903$ | | $m_{bk} = 31.9$ | $a = 0.2$ | $b = 2.5$ |
| $\omega_x = 6.0\,\pi$ | $\omega_y = 8.0\,\pi$ | $\omega_y = 3.0\,\pi$ | $I_{zb} = 259$ | |

*5.1. Stability Analysis by FM*

Twenty one cases of anisotropic rotor configurations are set out by taking into account the in-plane lead-lag natural frequency variation of the last blade ($\triangle\omega_{b4}$) from $-100\%$ to $+100\%$ by steps of 9% of the referential frequency described in Table 1.

For each configuration, the evolution of the multiplier characteristic as a function of rotor speed is computed from Eq.(6) and by considering the period divided into $p$=64 parts. The boundaries of instabilities are then determined and collected.

Repeating this procedure, the stability chart for the ground resonance phenomenon as a function of the asymmetry parameter $\triangle\omega_{b4}$ is obtained and shown in Figure 2. The unstable regions (with red lines) are defined between the symbols $\triangle$ and **O**.

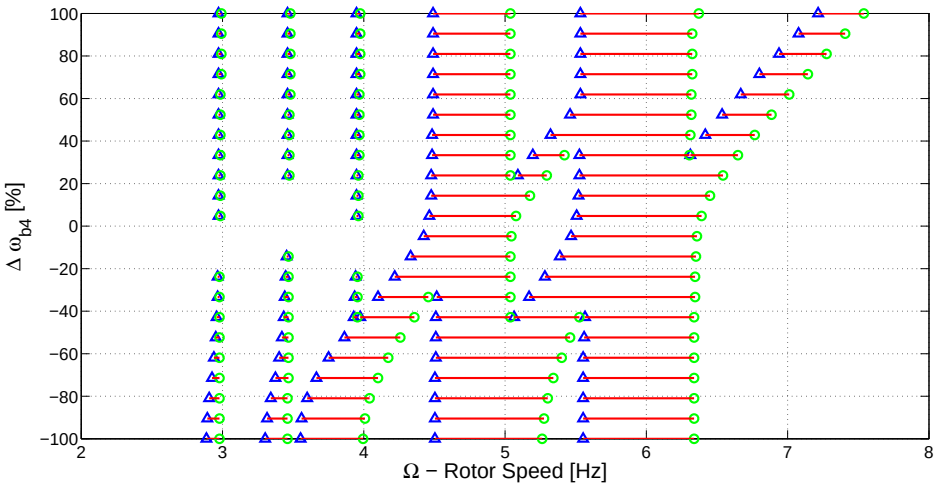


Figure 2: Stability chart for anisotropic rotor by taking into account the $4^{th}$ blade stiffness dissymmetric. Regions between $\triangle$ and **O** are unstable.

The result highlights the presence of two unstable regions that are not affect by the asymmetry on the rotor. They correspond to the same regions found in the isotropic rotor configuration $\triangle\omega_{b4} = 0\%$, and are located between rotor speed values ranging from 4.446 to 5.034 Hz and from 5.494 to 6.367 Hz. These instabilities happen due to the coalescence frequencies between fuselage and an asymmetric rotor mode shape (forward whirling mode) at a specific range of the rotor speed [16].

Moreover, it is noted that asymmetries higher than 15% cause the occurrence of new critical regions. Branches spread from the two zones mentioned above, creating new critical subregions. Also, unstable movements are also detected at rotor speeds around 3.0, 3.5 and 4.0 Hz which correspond to $\omega_1$, $\frac{(\omega_1+\omega_2)}{2}$ and $\omega_2$.

Nevertheless, small stiffness alterations ($|\triangle\omega_{b4}| < 15\%$) increases the distance between the boundary speeds, making the zones wider.

### *5.2. Stability Analysis by MMS*

A case of anisotropic rotors is set in order to compute a stability analysis with MMS. An arbitrary case is chosen from those studied in the previous sections, i.e. $\triangle\omega_{b4} = -40\%$.

The parametrically excited characteristic of the dynamical system and the expansions introduced by the perturbation method, highlight the presence of parametric resonances at first and/or second order equations. These resonances are illustrated graphically in Figure 3 which shows the evolution of the natural frequencies ($\omega_1$ to $\omega_6$) with the evolution of harmonic combinations at $\epsilon^1$ and $\epsilon^2$ order equations. They are plotted as a function of rotor speed $\Omega$.

The intersection points indicate resonant cases A to H and J to Q, and Table 2 contains the rotor speed values for all cases. Note that two resonances may occur simultaneously at the same rotor speed, which explains the use of lines connecting the points.

#### *5.2.1. Parametric resonant cases - $\epsilon^1$ equations*

The boundaries of ground resonance are determined by studying the stability of the solvability equations for each parametric resonant case. It is important to note that $\alpha_k = 1$ and $\beta_k = \frac{r_{b\,k}}{r_{m\,k}}$, for $k$=1..6, since the blades have the same geometrical and inertial properties.

- Case A - $\Omega_R = \omega_1 - \omega_{3..5} = 1.475 \times (2\pi)$

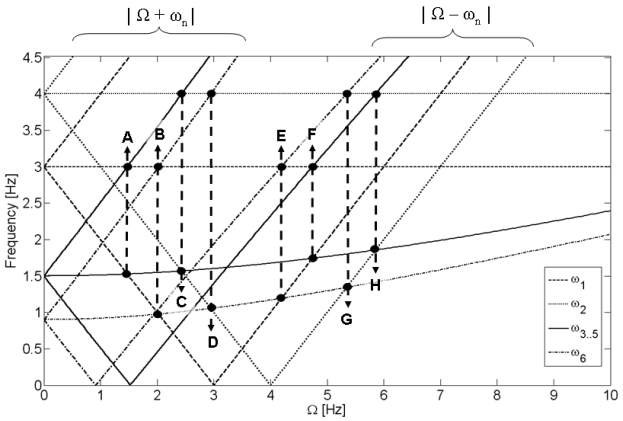


(a)

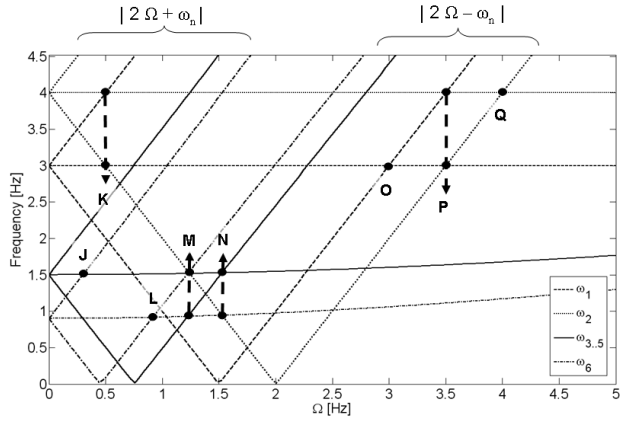


(b)

Figure 3: Evolution of harmonics combinations along with the evolution of natural frequencies for an anisotropic rotor: (a) at $\epsilon^{\mathbf{1}}$ equations and (b) at $\epsilon^{\mathbf{2}}$ equations

Table 2: Rotor speed values (Hz) of the parametric resonant cases found by MMS for an anisotropic rotor

| Resonant Cases of the First Order | | | | | | | |
|---|---|---|---|---|---|---|---|
| A | B | C | D | E | F | G | H |
| 1.475 | 2.02 | 2.433 | 2.94 | 4.192 | 4.741 | 5.343 | 5.855 |
| Resonant Cases of the Second Order | | | | | | | |
| J | K | L | M | N | O | P | Q |
| 0.299 | 0.500 | 0.916 | 1.223 | 1.526 | 3.000 | 3.500 | 4.000 |

The solvability equations are presented below:

$$-2\,I\,\omega_1\left(\frac{\partial}{\partial T_1}C_1\right)\mathrm{e}^{-I\sigma\,T_1}+\sum_{n=3}^{6}\frac{1}{2}\,I^{(n-2)}\alpha\,(\,\omega_n\,+\,\Omega_R)^2\,C_n=0 \tag{26}$$

$$2\,I\left(\frac{\partial}{\partial T_1}C_2\right)\omega_2=0 \tag{27}$$

$$-2\,I\,\omega_n\left(\frac{\partial}{\partial T_1}C_n\right)-\frac{1}{2}\,I^{(6-n)}\beta\,\omega_1^2\,C_1\mathrm{e}^{-I\sigma\,T_1}=0,\ n=3..5 \tag{28}$$

$$-2\,I\left(\frac{\partial}{\partial T_1}C_6\right)\omega_6=0 \tag{29}$$

The nonexistence of exciting terms at frequencies $\omega_2$ and $\omega_6$ explain why Eqs.(27) and (29) are homogeneous and independents. The amplitudes $C_n$ are functions of $T_1$ and $T_2$.

Differentiating Eq.(26) with respect to $T_1$ and replacing $\frac{\partial}{\partial T_1}C_k$, k =3..5 obtained from Eq.(28), a second order differential equation on $C_1$ is obtained.

Assuming $C_1 = (B_r + IB_i)\,\mathrm{e}^{(I\,\sigma\,T_1)}$, where $B_r$ and $B_i$ are real functions of $T_1$ and $T_2$, two new autonomous expressions are found once the real and imaginary terms are separated. They admit a nontrivial solution having the form $(B_r,\,B_i) = (b_r,\,b_i)\,\mathrm{e}^{(\Gamma T_1)}$ where $b_r$, $b_i$ and $\Gamma$ are constants.

By arranging them in matrix form, as a function of $b_r$ and $b_i$, the characteristic polynomial equation $P_A\,(\Gamma,\sigma)$ is then obtained as,

$$P_A\,(\Gamma,\sigma) = a_4\Gamma^4 + a_2\Gamma^2 + a_0 \tag{30}$$

where, $a_0 = -0.1905 \times 10^7$, $a_2 = -1423\sigma^2 - 0.329 \times 10^7$ and $a_4 = -1423$.

The polynomial characteristic equations of the remainder cases $P_k\,(\Gamma, \sigma)$, $k = \{B..H\}$ are found by repeating the procedure developed previously. They are not represented due to their volume and length.

The stability of the dynamical system is then determined by regarding the roots ($\Gamma$) of the characteristic polynomial equations. The system is stable when, by varying $\sigma$ over a certain range, the values of $\Gamma$ are all imaginary. This implies that $\Gamma^2$ should be real and negative. Figure 4 illustrates separately the evolution of the real and imaginary values of $\Gamma^2$ for all the parametric resonant cases of the first order with respect to the product $\epsilon\sigma$.

The results highlight that the ground resonance phenomenon appears only in the last four cases. The boundaries of instability, in Hz, range from -0.1425 to 0.1425 for case E, from -0.2042 to 0.2042 for case F and G, and, finally, from -0.3012 to 0.3012 for case H.

*5.2.2. Parametric resonant cases - $\epsilon^2$ equations*

Similar to the parametric resonant cases of the first order, the stability analysis of cases J to Q is carried out and the boundaries of instability are then predicted. Since the blades have the same geometrical and inertial properties, $\alpha_k = 1$ and $\beta_k = \frac{r_{b\,k}}{r_{m\,k}}$, for $k$=1..6.

The solvability equations can be represented as follows in all the resonant cases:

$$\frac{\partial}{\partial T_2}\begin{Bmatrix} C_1 \\ C_2 \end{Bmatrix} = \begin{bmatrix} v_{1,1} & v_{1,2} \\ v_{2,1} & v_{2,2} \end{bmatrix}\begin{Bmatrix} C_1 \\ C_2 \end{Bmatrix} + \begin{bmatrix} \overline{v}_{1,1} & \overline{v}_{1,2} \\ \overline{v}_{2,1} & \overline{v}_{2,2} \end{bmatrix}\begin{Bmatrix} \overline{C}_1 \\ \overline{C}_2 \end{Bmatrix} \tag{31}$$

$$\frac{\partial}{\partial T_2}\begin{Bmatrix} C_3 \\ \vdots \\ C_6 \end{Bmatrix} = \begin{bmatrix} v_{3,3} & \cdots & v_{3,6} \\ \vdots & \ddots & \vdots \\ v_{6,3} & \cdots & v_{6,6} \end{bmatrix}\begin{Bmatrix} C_3 \\ \vdots \\ C_6 \end{Bmatrix} + \begin{bmatrix} \overline{v}_{3,3} & \cdots & \overline{v}_{3,6} \\ \vdots & \ddots & \vdots \\ \overline{v}_{6,3} & \cdots & \overline{v}_{6,6} \end{bmatrix}\begin{Bmatrix} \overline{C}_3 \\ \vdots \\ \overline{C}_6 \end{Bmatrix} \tag{32}$$

Coefficients $v$ and $\overline{v}$ are given numerically. It should be noted that $\overline{C}$ is the conjugate term of $C$ and both are functions of $T_2$ only.

- Case J - $\Omega_R = \omega_{3..5} - \omega_6 = 0.299\ \times (2\pi)$

The coefficients values of Eqs.(31) and (32) are indicated below for the resonant case J.

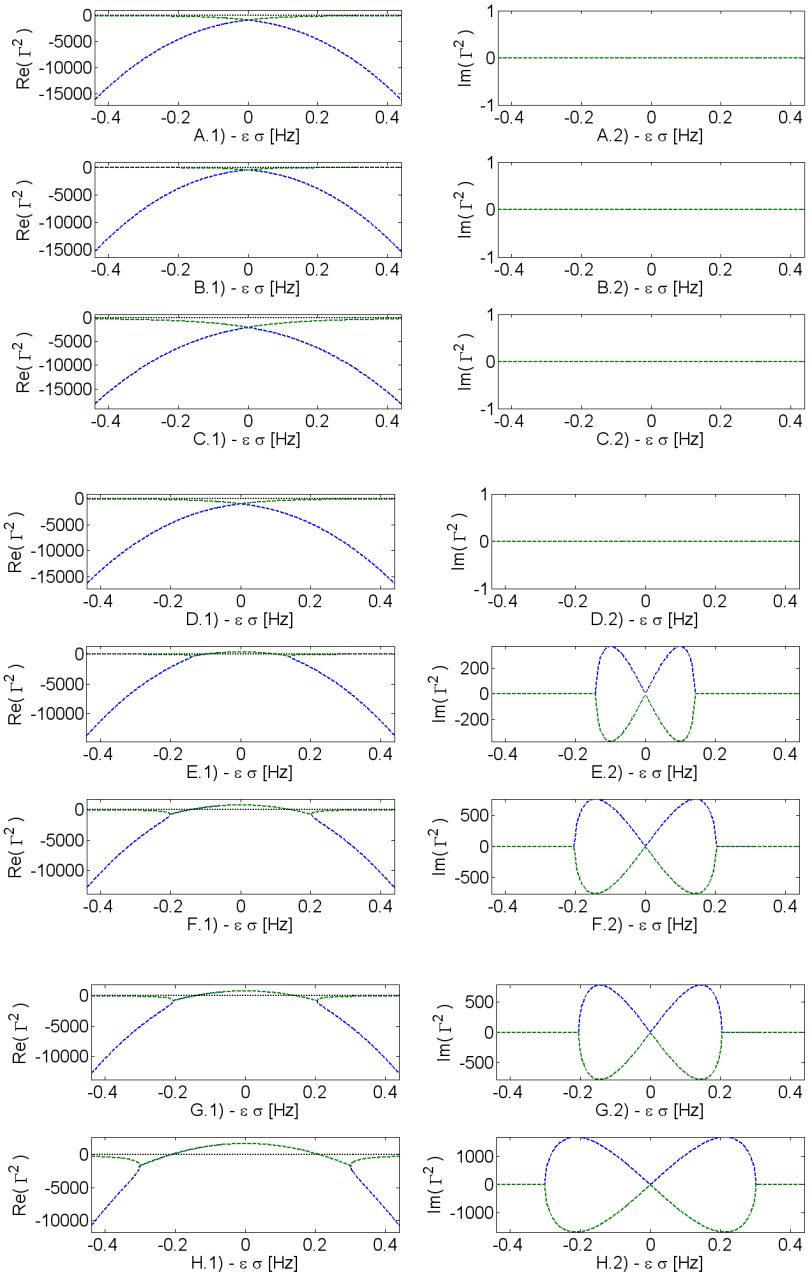


Figure 4: Stability analysis of the first order resonant cases A to H - 1) Evolution of the real part of $\Gamma^2$, 2) Evolution of the imaginary part of $\Gamma^2$

$$
\begin{array}{ll}
v_{1,1} = & 587.9\, I \\
v_{1,2} = & 0 \\
v_{3,3} = & -152.1\, I + 0.2804 \times 10^{-1}\, I\, \sigma \\
v_{3,5} = & 152.1\, I \\
v_{4,3} = & -152.1 \\
v_{4,5} = & 152.12 \\
v_{5,3} = & 152.14\, I \\
v_{5,5} = & 0.2804 \times 10^{-1}\, I\, \sigma - 152.1\, I \\
v_{6,3} = & 174.3 \mathrm{e}^{(2I\,\sigma\,T_2)} \\
v_{6,5} = & -174.3 \mathrm{e}^{(2I\,\sigma\,T_2)}
\end{array}
\qquad
\begin{array}{ll}
v_{2,2} = & 285.4\, I \\
v_{2,1} = & 0 \\
v_{3,4} = & 152.1 \\
v_{3,6} = & 0.1269 \times 10^{-2}\, \mathrm{e}^{(-2I\,\sigma\,T_2)} \\
v_{4,4} = & 0.2804 \times 10^{-1}\, I\, \sigma - 152.13\, I \\
v_{4,6} = & 0.1269 \times 10^{-2}\, I\, \mathrm{e}^{(-2I\,\sigma\,T_2)} \\
v_{5,4} = & -152.1 \\
v_{5,6} = & 0.1269 \times 10^{-2}\, \mathrm{e}^{(-2I\,\sigma\,T_2)} \\
v_{6,4} = & 174.3\, I\, \mathrm{e}^{(2I\,\sigma\,T_2)} \\
v_{6,6} = & 0.4583 \times 10^{-1}\, I\, \sigma - 37.96\, I
\end{array}
$$

Two sets of autonomous equations are obtained once $C_k = (B_{r\,k} + IB_{i\,k})\, \mathrm{e}^{(I\,\sigma\,T_2)}$ for $k = \{1, 2, 6\}$, and $C_k = (B_{r\,k} + IB_{i\,k})\, \mathrm{e}^{(-I\,\sigma\,T_2)}$ for $k$=3..5 in Eqs. (31) and (32). The variables $B_{r\,k}$ and $B_{i\,k}$ are real functions of $T_2$. They admit non-trivial solutions having the form $[B_{r\,k},\, B_{i\,k}] = [d_{r\,k}, d_{i\,k}]\, \mathrm{e}^{(\Gamma T_1)}$ where $\Gamma$, $d_{r\,k}$ and $d_{i\,k}$ are constants.

Arranging them in a matrix form as a function of $d_{r\,k}$ and $d_{i\,k}$, the polynomial characteristic equations $P_{J,1}\,(\Gamma, \sigma)$ and $P_{J,2}\,(\Gamma, \sigma)$, originated from Eqs. (31) and (32) in that order and expressed as a function of $\Gamma$ and $\sigma$, are:

$$
P_{J,1}\,(\Gamma, \sigma) = \Gamma^4 + a_2^1 \Gamma^2 + a_0^1 \tag{33}
$$

$$
P_{J,2}\,(\Gamma, \sigma) = \Gamma^8 + a_6^2 \Gamma^6 + a_4^2 \Gamma^4 + a_2^2 \Gamma^2 + a_0^2 \tag{34}
$$

where,

$$
\begin{aligned}
a_0^1 &= \sigma^4 - 722.2\, \sigma^3 + 0.1953 \times 10^6\, \sigma^2 - 0.2343 \times 10^8\, \sigma + 0.1052 \times 10^{10} \\
a_2^1 &= 2\, \sigma^2 - 722.2\, \sigma + 0.6553 \times 10^5 \\
a_0^2 &= \begin{array}{c} \sigma^8 + 58.64\, \sigma^7 + 912.0\, \sigma^6 + 1045\, \sigma^5 - 0.1371 \times 10^5\, \sigma^4 + ... \\ -0.1286 \times 10^5\, \sigma^3 + 0.6024 \times 10^5\, \sigma^2 - 6.0 \times 10^{-12}\, \sigma + 1.607 \times 10^{-11} \end{array} \\
a_2^2 &= 4\, \sigma^6 + 175.9\, \sigma^5 + 2635\, \sigma^4 + 4260\, \sigma^3 + 4204\, \sigma^2 - 0.1286 \times 10^5\, \sigma + 0.6024 \times 10^5 \\
a_4^2 &= 6\, \sigma^4 + 175.9\, \sigma^3 + 2535 \sigma^2 + 3214\, \sigma + 0.1791 \times 10^5 \\
a_6^2 &= 4\, \sigma^2 + 58.64\, \sigma + 811.4
\end{aligned}
$$

Previous coefficients are the results of numerical application from Table 1 of which the analytical expressions are not presented in this paper. The

polynomial characteristic equations of remainder resonant cases $P_k(\Gamma, \sigma)$, $k = \{\text{K..Q}\}$, are achieved by following the same actions described previously.

By conforming to the same criteria as those established in section 5.2.1, stability is determined by considering the roots ($\Gamma$) of the characteristic polynomial equations. Figure 5 illustrates separately the evolution of the real and imaginary parts of $\Gamma^2$ with respect now to the product $\epsilon^2\sigma$.

The analysis indicates unstable oscillations from -0.0288 to 0.0171 Hz for case O, from -0.0534 to -0.0325 Hz for case P, and from -0.0592 to -0.038 Hz for the last case Q.

With respect to case N, when regarding the amplitudes of the imaginary terms, it can be seen that they are smaller than the real ones. The real part of the exponent obtained for the helicopter responses can be neglected, once the square root has been extracted (passing from $\Gamma^2$ to $\Gamma$) and multiplied by $\epsilon^2$ (passing from $T_2$ to $t$), leading to small values ($\sim 1 \times 10^{-6}$). Finally, resonant case N presents stable oscillations.

Comparing the results obtained from FM and MMS in Table 3 highlights the predicted boundary speeds of the ground resonance phenomenon. There are seven instability zones: the last four correspond to parametrical resonances of the first order and the three first are unstable parametric resonances of the second order.

The shifts between both methods are calculated by taking into account the mean rotor speed values at each zone.

Table 3: Limits of instability zones predicted by using FM and MMS for an anisotropic rotor configuration with $\triangle\omega_{b4} = -40\%$ and the shift between the mean critical rotor speed values

| Resonant Case | FM | | MMS | | Error [%] |
|---|---|---|---|---|---|
| 1 / O | 2.959 | 2.979 | 2.971 | 2.983 | 0.27 |
| 2 / P | 3.348 | 3.462 | 3.447 | 3.467 | 0.20 |
| 3 / Q | 3.933 | 3.956 | 3.941 | 3.962 | 0.18 |
| 4 / E | 4.016 | 4.384 | 4.049 | 4.335 | 0.97 |
| 5 / F | 4.516 | 5.039 | 4.537 | 4.945 | 1.17 |
| 6 / G | 5.096 | 5.545 | 5.139 | 5.547 | 0.44 |
| 7 / H | 5.568 | 6.339 | 5.554 | 6.156 | 1.57 |

Regarding in details into the three specific unstable regions (cases P,

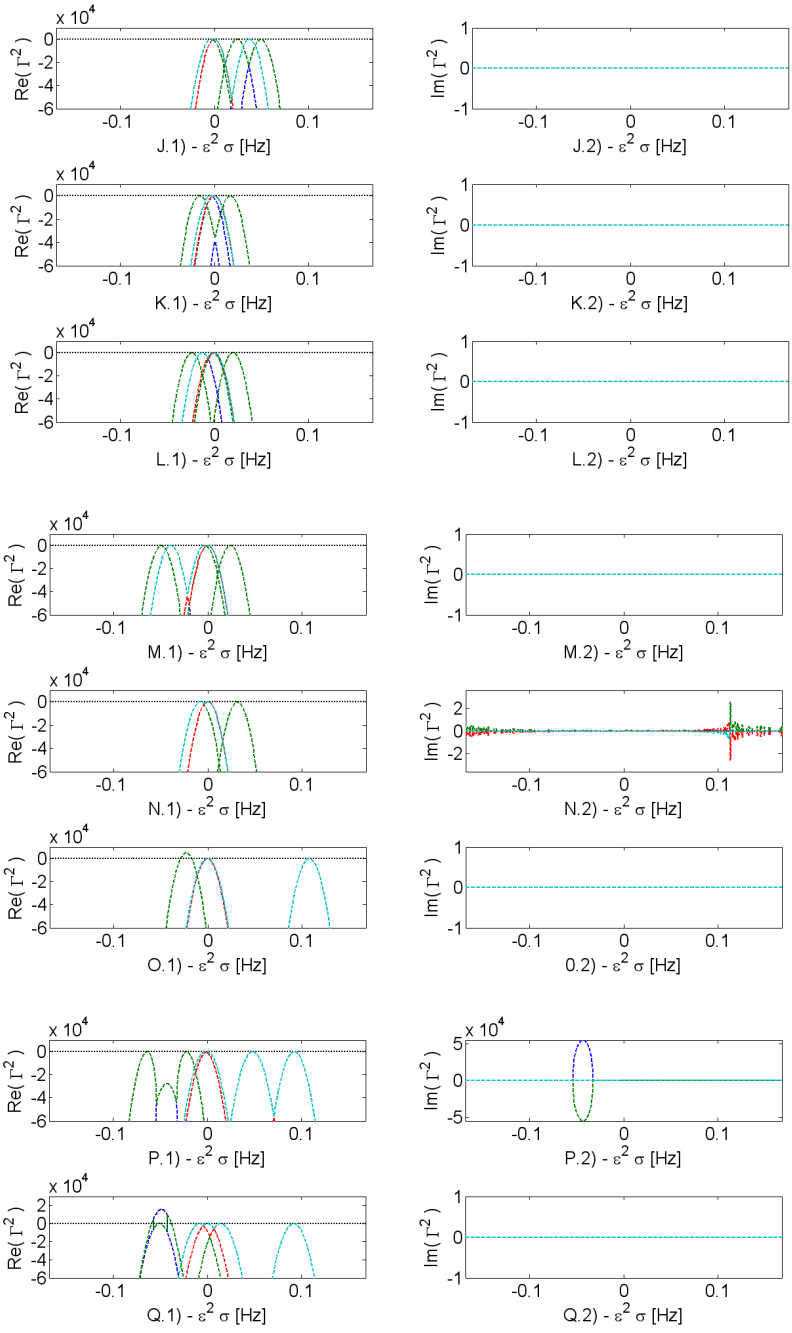


Figure 5: Stability analysis of the second order resonant cases J to Q - 1) Evolution of the real part of $\Gamma^2$, 2) Evolution of the imaginary part of $\Gamma^2$

E and H), Figure 6 shows the deformation shapes of the helicopter at the instants of the maximal amplitude displacement of the fuselage. The amplitude of movements are obtained from temporal responses, computed through a numerical step-by-step integration method (see Appendix B).

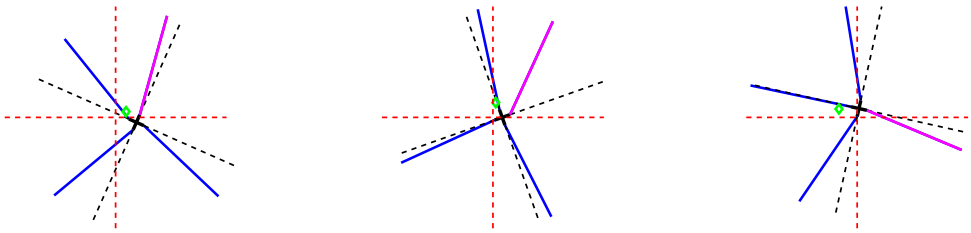

(a) Case P (b) Case E (c) Case H

Figure 6: Rotor Deformation of an Helicopter with one Dissimilar Blade (pink line) - $\Delta\omega_{b4} = -40\%$ -, during time integration at a given time step, with: (a) $\Omega = 3.45Hz$ - Case P, (b) $\Omega = 4.20Hz$ - Case E and (c) $\Omega = 5.91Hz$ - Case H. The green point denotes the instantaneous centre of gravity of the blades.

The intersection point between two dashed red lines corresponds to the rest point of the helicopter and the dashed black lines indicate the level zero of blade lead-lag oscillations. The pink line represents the dissimilar blade and the green diamond symbol indicates the position of the rotor center of mass. In order to help the comprehension and the visualization of Figure 6a, the amplitudes are multiplied by 500.

The rotor center of mass are shifted from the axis of rotation in all cases, indicating the presence of a non symmetric rotor deformation. Moreover, from the temporal responses at a given time, the amplitudes of movement reached by the blades and fuselage in cases E and H (i.e.: instabilities at first order) are higher than those obtained in P (i.e.: instability at second order).

Moreover, in case P, the longitudinal and lateral displacements of the fuselage have the same amplitude level (see Figure B.7). Through the analysis obtained by MMS, this fact is explained by the presence of parametric resonance involving both displacements of the fuselage, as verified by the case P in the Figure 3b.

Regarding the case E in Figure 3a, the longitudinal displacement of the fuselage and the lead-lag oscillation of the perturbed blade are in resonance

(evidenced by highest amplitude of $u_1$ and $u_6$ in Figure B.8). The same analysis for case H highlights the high correspondence between the temporal results and those obtained by the MMS.

## 6. Conclusion

In recent decades, helicopter stability (e.g. the ground resonance phenomenon) has attracted much attention. Predicting the critical rotor speeds at which the phenomenon occurs for isotropic and anisotropic rotor configurations has been studied and the influence of small in-plane stiffness asymmetries between blades analyzed.

The equations of motions were simplified and the instability regions easily identified for the isotropic rotor configuration. However, anisotropic rotor configuration requires considering and treating periodical equations of motions. Floquet's Method (FM) has been used frequently to determine the boundaries of instability in this kind of rotor.

The aim of the present work was to verify the influence of high in-plane stiffness variation at one blade on stability, specifically the ground resonance phenomenon. To do this, the classical FM was used and the Method of Multiple Scales (MMS) was proposed.

With the latter method, the helicopter, considered as a parametrically excited system, leads to the occurrence of periodic terms of high order $\epsilon$ equations. In our case we focused on the advantages of using methods that give analytical responses (i.e, versatility and less CPU time) and on determining the existence of parametric resonances capable of explaining ground resonance in helicopters. The stability analysis on each of these resonances led to the identification of critical regions and identifying their boundary speeds.

By performing a numerical analysis and using FM, a complex stability chart was obtained that illustrated the evolution of the instability boundaries of different anisotropic rotors as a function of rotor speed. The asymmetry was introduced by varying the in-plane lead-lag natural frequency of one blade from -100% to +100%. The occurrence of new instability zones was detected for an in-plane lead-lag variation higher than $\pm 15\%$.

However, with MMS, the treatment of a parametrically excited system led to the identification of sixteen parametric resonant cases, of which seven were identified as exponentially unstable. They were linked to the existence

of parametric instabilities and expressed as a combination of blade and/or fuselage natural frequencies.

Great similarity between the results could be seen when comparing the instability boundaries established with MMS and those with FM (considering the same asymmetry case). A temporal analysis of the periodical equations of motions highlight the exponential evolution of the amplitude of oscillation at three instability regions, beyond the good correspondence with the results obtained with the MMS.

The prediction of the ground resonance phenomenon was easily and accurately obtained by using MMS. For each resonant case, studying the evolution of the roots of an analytical expression (i.e. the polynomial characteristic equation), led to identifying the critical regions. Furthermore, it improved understanding of the existence of certain instability regions in the stability chart. The unstable regions at low rotor speed values corresponded to parametric instabilities of the second order, whereas the others were parametric instabilities of the first order.

## Appendix A. Responses of $u_{n_1}$

The responses $u_{n_1}$ for a non-resonant case at order $\epsilon^1$ set of equations are illustrated as:

$$
\begin{aligned}
u_{1_1} = \\
&\frac{1}{2}\left(\frac{-i\left(\Omega+\omega_3\right)^2\alpha\,\mathrm{e}^{i(\Omega+\omega_3)T_0}}{\left(\omega_1+\Omega+\omega_3\right)\left(-\omega_1+\Omega+\omega_3\right)}+\frac{i\alpha\,\mathrm{e}^{-i(\Omega-\omega_3)T_0}\left(\Omega-\omega_3\right)^2}{\left(-\omega_1+\Omega-\omega_3\right)\left(\omega_1+\Omega-\omega_3\right)}\right)C_3\\
&+\frac{1}{2}\left(\frac{\alpha\,\left(\Omega-\omega_4\right)^2\mathrm{e}^{-i(\Omega-\omega_4)T_0}}{\left(-\omega_1+\Omega-\omega_4\right)\left(\omega_1+\Omega-\omega_4\right)}+\frac{\alpha\,\left(\Omega+\omega_4\right)^2\mathrm{e}^{i(\Omega+\omega_4)T_0}}{\left(\omega_1+\Omega+\omega_4\right)\left(-\omega_1+\Omega+\omega_4\right)}\right)C_4\\
&+\frac{1}{2}\left(\frac{-i\mathrm{e}^{-i(\Omega-\omega_5)T_0}\left(\Omega-\omega_5\right)^2\alpha}{\left(-\omega_1+\Omega-\omega_5\right)\left(\omega_1+\Omega-\omega_5\right)}+\frac{i\mathrm{e}^{i(\Omega+\omega_5)T_0}\alpha\,\left(\Omega+\omega_5\right)^2}{\left(\omega_1+\Omega+\omega_5\right)\left(-\omega_1+\Omega+\omega_5\right)}\right)C_5\\
&+\frac{1}{2}\left(-\frac{\alpha\,\left(\Omega-\omega_6\right)^2\mathrm{e}^{-i(\Omega-\omega_6)T_0}}{\left(-\omega_1+\Omega-\omega_6\right)\left(\omega_1+\Omega-\omega_6\right)}-\frac{\alpha\,\left(\Omega+\omega_6\right)^2\mathrm{e}^{i(\Omega+\omega_6)T_0}}{\left(\omega_1+\Omega+\omega_6\right)\left(-\omega_1+\Omega+\omega_6\right)}\right)C_6\\
&+[c.c.]
\end{aligned}
\tag{A.1}
$$

$$
\begin{aligned}
u_{2_1} = & \\
& \frac{1}{2}\left(-\frac{\left(\Omega+\omega_3\right)^2\alpha\,\mathrm{e}^{i(\Omega+\omega_3)T_0}}{\left(\omega_2+\Omega+\omega_3\right)\left(-\omega_2+\Omega+\omega_3\right)}-\frac{\alpha\,\left(\Omega-\omega_3\right)^2\mathrm{e}^{-i(\Omega-\omega_3)T_0}}{\left(-\omega_2+\Omega-\omega_3\right)\left(\omega_2+\Omega-\omega_3\right)}\right)C_3 \\
& +\frac{1}{2}\left(\frac{-i\alpha\,\left(\Omega+\omega_4\right)^2\mathrm{e}^{i(\Omega+\omega_4)T_0}}{\left(\omega_2+\Omega+\omega_4\right)\left(-\omega_2+\Omega+\omega_4\right)}+\frac{i\alpha\,\left(\Omega-\omega_4\right)^2\mathrm{e}^{-i(\Omega-\omega_4)T_0}}{\left(-\omega_2+\Omega-\omega_4\right)\left(\omega_2+\Omega-\omega_4\right)}\right)C_4 \\
& +\frac{1}{2}\left(\frac{\alpha\,\left(\Omega+\omega_5\right)^2\mathrm{e}^{i(\Omega+\omega_5)T_0}}{\left(\omega_2+\Omega+\omega_5\right)\left(-\omega_2+\Omega+\omega_5\right)}+\frac{\alpha\,\left(\Omega-\omega_5\right)^2\mathrm{e}^{-i(\Omega-\omega_5)T_0}}{\left(-\omega_2+\Omega-\omega_5\right)\left(\omega_2+\Omega-\omega_5\right)}\right)C_5 \\
& +\frac{1}{2}\left(\frac{-i\mathrm{e}^{-i(\Omega-\omega_6)T_0}\alpha\,\left(\Omega-\omega_6\right)^2}{\left(-\omega_2+\Omega-\omega_6\right)\left(\omega_2+\Omega-\omega_6\right)}+\frac{i\mathrm{e}^{i(\Omega+\omega_6)T_0}\alpha\,\left(\Omega+\omega_6\right)^2}{\left(\omega_2+\Omega+\omega_6\right)\left(-\omega_2+\Omega+\omega_6\right)}\right)C_6 \\
& +[c.c.]
\end{aligned}
\tag{A.2}
$$

$$
\begin{aligned}
u_{3_1} = & \\
& \frac{1}{2}\left(\frac{-i\beta\,\omega_1^2\mathrm{e}^{i(\Omega+\omega_1)T_0}}{\left(\omega_1+\Omega+\omega_3\right)\left(\omega_1+\Omega-\omega_3\right)}+\frac{i\beta\,\omega_1^2\mathrm{e}^{-i(\Omega-\omega_1)T_0}}{\left(-\omega_1+\Omega-\omega_3\right)\left(-\omega_1+\Omega+\omega_3\right)}\right)C_1 \\
& +\frac{1}{2}\left(-\frac{\beta\,\omega_2^2\,\mathrm{e}^{-i(\Omega-\omega_2)T_0}}{\left(-\omega_2+\Omega-\omega_3\right)\left(-\omega_2+\Omega+\omega_3\right)}-\frac{\beta\,\omega_2^2\,\mathrm{e}^{i(\Omega+\omega_2)T_0}}{\left(\omega_2+\Omega+\omega_3\right)\left(\omega_2+\Omega-\omega_3\right)}\right)C_2 \\
& +[c.c.]
\end{aligned}
\tag{A.3}
$$

$$
\begin{aligned}
u_{4_1} = & \\
& \frac{1}{2}\left(\frac{\beta\,\omega_1^2\,\mathrm{e}^{i(\Omega+\omega_1)T_0}}{\left(\omega_1+\Omega+\omega_4\right)\left(\omega_1+\Omega-\omega_4\right)}+\frac{\beta\,\omega_1^2\,\mathrm{e}^{-i(\Omega-\omega_1)T_0}}{\left(-\omega_1+\Omega-\omega_4\right)\left(-\omega_1+\Omega+\omega_4\right)}\right)C_1 \\
& +\frac{1}{2}\left(\frac{i\beta\,\omega_2^2\,\mathrm{e}^{-i(\Omega-\omega_2)T_0}}{\left(-\omega_2+\Omega-\omega_4\right)\left(-\omega_2+\Omega+\omega_4\right)}-\frac{i\beta\,\omega_2^2\,\mathrm{e}^{i(\Omega+\omega_2)T_0}}{\left(\omega_2+\Omega+\omega_4\right)\left(\omega_2+\Omega-\omega_4\right)}\right)C_2 \\
& +[c.c.]
\end{aligned}
\tag{A.4}
$$

$$
\begin{aligned}
u_{5_1} = & \\
& \frac{1}{2}\left(\frac{i\beta\,\omega_1^2\,\mathrm{e}^{i(\Omega+\omega_1)T_0}}{(\omega_1+\Omega+\omega_5)\,(\omega_1+\Omega-\omega_5)} - \frac{i\beta\,\omega_1^2\,\mathrm{e}^{-i(\Omega-\omega_1)T_0}}{(-\omega_1+\Omega-\omega_5)\,(-\omega_1+\Omega+\omega_5)}\right) C_1 \\
& + \frac{1}{2}\left(\frac{\beta\,\omega_2^2\,\mathrm{e}^{-i(\Omega-\omega_2)T_0}}{(-\omega_2+\Omega-\omega_5)\,(-\omega_2+\Omega+\omega_5)} + \frac{\beta\,\omega_2^2\,\mathrm{e}^{i(\Omega+\omega_2)T_0}}{(\omega_2+\Omega+\omega_5)\,(\omega_2+\Omega-\omega_5)}\right) C_2 \\
& + [c.c.]
\end{aligned}
\tag{A.5}
$$

$$
\begin{aligned}
u_{6_1} = & \\
& \frac{1}{2}\left(-\frac{\beta\,\omega_1^2\,\mathrm{e}^{i(\Omega+\omega_1)T_0}}{(\omega_1+\Omega+\omega_6)\,(\omega_1+\Omega-\omega_6)} - \frac{\beta\,\omega_1^2\,\mathrm{e}^{-i(\Omega-\omega_1)T_0}}{(-\omega_1+\Omega-\omega_6)\,(-\omega_1+\Omega+\omega_6)}\right) C_1 \\
& + \frac{1}{2}\left(\frac{-i\beta\,\omega_2^2\,\mathrm{e}^{-i(\Omega-\omega_2)T_0}}{(-\omega_2+\Omega-\omega_6)\,(-\omega_2+\Omega+\omega_6)} + \frac{i\beta\,\omega_2^2\,\mathrm{e}^{i(\Omega+\omega_2)T_0}}{(\omega_2+\Omega+\omega_6)\,(\omega_2+\Omega-\omega_6)}\right) C_2 \\
& + [c.c.]
\end{aligned}
\tag{A.6}
$$

## Appendix B. Temporal Responses

The numerical step-by-step integration method "Adams113", in MATLAB ®, is used to compute the temporal responses of a helicopter with one dissymmetric blade $\Delta\omega_{b4} = -40\%$ at three critical regions (cases P, E and H). The rotating speed value considered for the analyses are, in Hz, equal to 3.45, 4.20 and 5.91, respectively.

The initial conditions imposed are $0.1^\circ$ for the lead-lag oscillation of $4^{th}$ blade, and zero for all remainder amplitudes and speeds.

Figures B.7 to B.9 illustrate the results obtained at the regions defined by cases P, E and H, respectively.

## References


[1] A. Nayfeh, *Perturbation methods*, vol. 6. Wiley Online Library, 1973.

[2] A. Nayfeh and D. Mook, *Nonlinear oscillations*, vol. 31. Wiley Online Library, 1979.

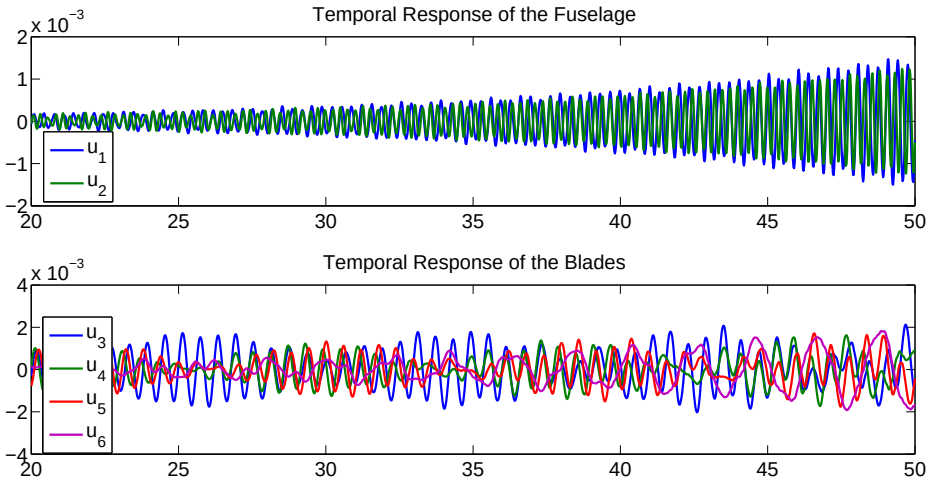


Figure B.7: Temporal Response of the Fuselage and Blades of an Helicopter with one Dissimilar Blade - $\Delta\omega_{b4} = -40\%$ - at Case P with $\Omega = 3.45Hz$

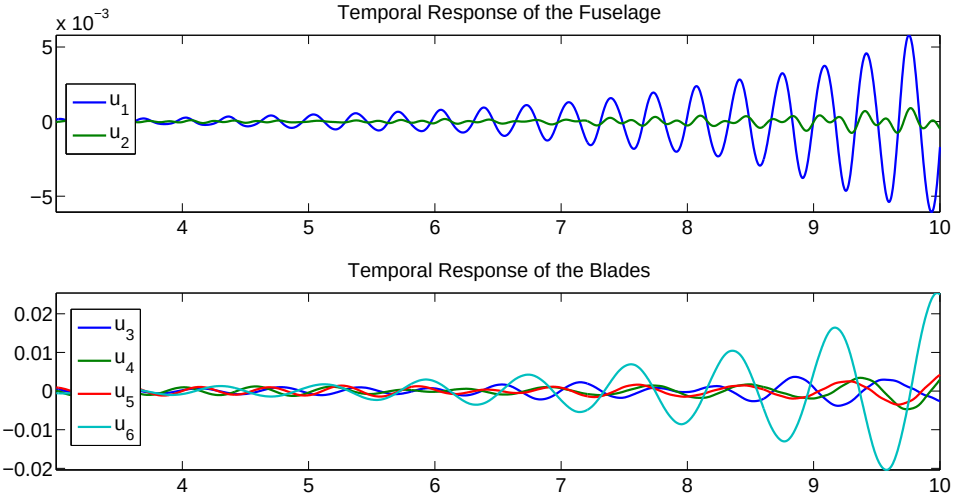


Figure B.8: Temporal Response of the Fuselage and Blades of an Helicopter with one Dissimilar Blade - $\Delta\omega_{b4} = -40\%$ - at Case E with $\Omega = 4.20Hz$

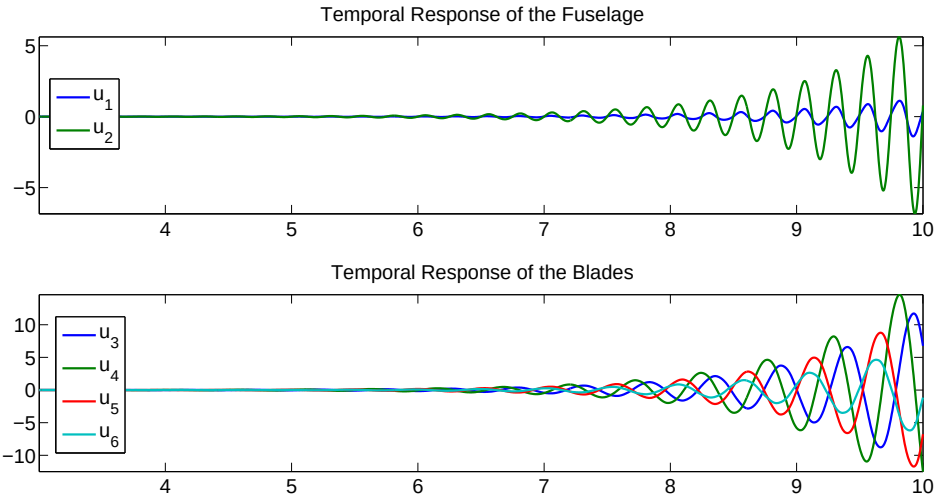


Figure B.9: Temporal Response of the Fuselage and Blades of an Helicopter with one Dissimilar Blade - $\Delta\omega_{b4} = -40\%$ - at Case H with $\Omega = 5.91Hz$


[3] N. Driot, C. Lamarque, and A. Berlioz, "Theoretical and Experimental Analysis of a Base-Excited Rotor," *Journal of Computational and Nonlinear Dynamics*, vol. 1, p. 257, 2006.

[4] M. Duchemin, A. Berlioz, and G. Ferraris, "Dynamic Behavior and stability of a rotor under base excitation," *Journal of Vibration and Acoustics*, vol. 128, p. 576, 2006.

[5] M. R. Shad, G. Michon, and A. Berlioz, "Modeling and analysis of nonlinear rotordynamics due to higher order deformations in bending," *Applied Mathematical Modelling*, vol. 35, no. 5, pp. 2145 – 2159, 2011.

[6] G. Michon, L. Manin, R. Parker, and R. Dufour, "Duffing oscillator with parametric excitation: analytical and experimental investigation on a belt-pulley system," *Journal of Computational and Nonlinear Dynamics*, vol. 3, p. 031001, 2008.

[7] A. O. Belyakov, A. P. Seyranian, and A. Luongo, "Dynamics of the pendulum with periodically varying length," *Physica D: Nonlinear Phenomena*, vol. 238, no. 16, pp. 1589 – 1597, 2009.

[8] A. Seyranian and A. Seyranian, "The stability of an inverted pendulum with a vibrating suspension point," *Journal of Applied Mathematics and Mechanics*, vol. 70, no. 5, pp. 754 – 761, 2006.

[9] X. Xu and M. Wiercigroch, "Approximate analytical solutions for oscillatory and rotational motion of a parametric pendulum," *Nonlinear Dynamics*, vol. 47, no. 1, pp. 311–320, 2007.

[10] R. Coleman and A. Feingold, "Theory of self-excited mechanical oscillations of helicopter rotors with hinged blades," Tech. Rep. Report 1351, NACA Techinical Note 3844, 1957.

[11] R. Donham, S. Cardinale, and I. Sachs, "Ground and Air Resonance Characteristics of a Soft In-Plane Rigid-Rotor System," *Journal of the American Helicopter Society*, vol. 14, p. 33, 1969.

[12] D. Hodges, "An aeromechanical stability analysis for bearingless rotor helicopters," *Journal of the American Helicopter Society*, vol. 24, p. 2, 1979.

[13] R. Lytwyn, W. Miao, and W. Woitsch, "Airborne and ground resonance of hingeless rotors," *Journal of the American Helicopter Society*, vol. 16, p. 2, 1971.

[14] C. Robinson, R. King, and E. Wood, "Non-linear simulation of coupled rotor-fuselage response using symbolically derived equations of motion. Part 1: derivation," *Proceedings of the Institution of Mechanical Engineers, Part G: Journal of Aerospace Engineering*, vol. 218, no. 1, pp. 1–9, 2004.

[15] C. Robinson, R. King, and E. Wood, "Non-linear simulation of coupled rotor-fuselage response using symbolically derived equations of motion. Part 2: confirmation and illustrative cases," *Proceedings of the Institution of Mechanical Engineers, Part G: Journal of Aerospace Engineering*, vol. 218, no. 1, pp. 11–22, 2004.

[16] J. Wang and I. Chopra, "Dynamics of helicopters in ground resonance with and without blade dissimilarities," in *AIAA Dynamics Specialists Conference, Dallas, TX*, pp. 273–291, 1992.

[17] C. Hammond, "An application of Floquet theory to prediction of mechanical instability," *Journal of the American Helicopter Society*, vol. 19, p. 14, 1974.

[18] L. Sanches, G. Michon, A. Berlioz, and D. Alazard, "Modélisation Dynamique d'un Rotor sur Base Flexible (Dynamic Modeling of a Rotor Over a Flexible Base)," in *Congress Français de Mécanique, 24-28 August, Marseille*, 2009.

[19] P. Skjoldan and M. Hansen, "On the similarity of the Coleman and Lyapunov-Floquet transformations for modal analysis of bladed rotor structures," *Journal of Sound and Vibration*, vol. 327, no. 3-5, pp. 424–439, 2009.

[20] R. Dufour and A. Berlioz, "Parametric instability of a beam due to axial excitations and to boundary conditions," *Journal of Vibration and Acoustics*, vol. 120, no. 2, pp. 461–467, 1998.

**List of Figures**



**List of Tables**